Observed and CMIP6 model simulated organic aerosol response to drought in the contiguous United States during summertime

Wei Li[1,2] and Yuxuan Wang[1]

[1]Department of Earth and Atmospheric Sciences, University of Houston, Houston, Texas, USA

[2]Now at Cooperative Institute for Satellite Earth System Studies, George Mason University, Fairfax, Virginia, USA

Corresponding author: Yuxuan Wang (ywang246@central.uh.edu)

Abstract. Drought events have been linked with the enhancements of organic aerosols (OA), but the mechanisms have not been comprehensively understood. This study investigates the relationships between the monthly standardized precipitation–evapotranspiration index (SPEI) and surface OA in the contiguous United States (CONUS) during the summertime from 1998 to 2018. OA under severe drought conditions shows a significant increase in mass concentrations across most of the CONUS relative to non-drought periods with the Pacific Northwest (PNW) and Southeastern United States (SEUS) experiencing the highest average enhancement of 1.79 μg m^{-3} (112 %) and 0.92 μg m^{-3} (33 %), respectively. In the SEUS, a linear regression approach between OA and sulfate was used to estimate the epoxydiols-derived secondary organic aerosol (IEPOX SOA), which is the primary driver of the OA enhancements under droughts due to the simultaneous increase in biogenic volatile organic compounds (VOCs; such as isoprene and monoterpene) emissions and sulfate. The rise of sulfate is mainly caused by the reduced wet deposition because of the up to 62% lower precipitation amount. In the PNW, OA enhancements are closely linked to intensified wildfire emissions, which raise OA mass concentrations to be four to eight times higher relative to non-fire conditions. All ten Earth system models participating in the sixth phase of the Coupled Model Intercomparison Project (CMIP6) can capture the slopes between SPEI and OA in the PNW with CESM2-WACCM and GFDL-ESM4 performing the best and worst in predicting the OA enhancement under severe droughts. However, all models significantly underestimate the OA increase in the SEUS with Nor-ESM2-LM and MIRCO6 showing relatively better performance. This study reveals the key drivers of the elevated OA levels under droughts in the CONUS and underscores the deficiencies of current climate models in their predictive capacity for assessing the impact of future droughts on air quality.

1. Introduction

Drought events, marked by prolonged periods of water scarcity and precipitation deficits, have profound impacts on the hydrological cycle, ecosystems, and society (Wilhite et al., 2007). The contiguous United States (CONUS) is especially prone to droughts, and recent years have witnessed an escalation in both the frequency and severity of drought episodes across various regions (Leeper et al., 2022; Strzepek et al., 2010). These drought events are intricately linked to the modifications in atmospheric processes, such as emission, production, transport, and deposition, which can extend beyond the immediate hydrological impacts with far-reaching implications for air

quality. Specifically, organic aerosol (OA), a major component of the particulate matter with an aerodynamic diameter less than or equal to 2.5 μm ($PM_{2.5}$), emerges as a critical air quality concern influenced by the complex interactions between drought-induced meteorological conditions and biogeochemical processes.

OA can be directly emitted into the atmosphere through combustion activities, such as transportation fuel and biomass burning. This kind of OA is called primary organic aerosol (POA), whereas secondary organic aerosol (SOA) is produced by the oxidation of volatile organic compounds (VOCs). The intricate interplay between drought and OA dynamics involves complex feedback mechanisms. Biogenic isoprene, mainly emitted by terrestrial vegetation, is an important precursor of SOA and is highly sensitive to drought conditions. Both laboratory and field measurements have shown that biogenic emissions of isoprene will increase at the initial stage of drought development primarily due to temperature stimulus but drop eventually under prolonged severe drought limited by soil water availability (Pegoraro et al., 2005; Brilli et al., 2007; Potosnak et al., 2014). The abnormally high temperature and low humidity under droughts can enhance the oxidation of OA (Maria et al., 2004; Yli-Juuti et al., 2021), while low cloud water content lowers the aqueous SOA formation (Brégonzio-Rozier et al., 2016; Tsui et al., 2019), leading to compensating changes in the mass and hygroscopicity of OA. Aerosols are most effectively removed by wet scavenging, which will be reduced under lower rainfall intensity and frequency (Dawson et al., 2007; Fang et al., 2011). In addition, dry conditions can trigger large and high-intensity wildfires, emitting more POA and VOC precursors into the atmosphere (Ruffault et al., 2018; Taufik et al., 2017). The interactions of these factors underscore the need for a comprehensive understanding of the mechanisms driving variations in OA during drought events.

OA, due to its fine particulate nature and diverse chemical composition, exerts significant adverse effects on climate and human health. OA is found to be associated with a higher county-level cardiorespiratory mortality rate than other major $PM_{2.5}$ components, such as sulfate, ammonium, and nitrate (Pye et al., 2021). OA can scatter solar radiation, form cloud condensation nuclei, and affect cloud droplet concentrations, posing big uncertainties on radiative forcing and climate feedback (Carslaw et al., 2013; Lee et al., 2016). The coupled chemistry-climate models and Earth system models (ESMs) are fundamental tools for studying global warming and the accuracy of OA simulations in these models are crucial constraints on their credibility in climate change simulation and projection (Gomez et al., 2023; Thornhill et al., 2021). The Coupled Model Intercomparison Project Phase 6 (CMIP6), containing the new generation of ESMs with interactive aerosol and gas chemistry implemented (Turnock et al., 2020), provides a valuable opportunity to evaluate the simulated OA and its response to drought, which is projected to be more frequent in the future (Cook et al., 2018)

Several case studies have focused on the impacts of droughts on the concentrations and speciation of $PM_{2.5}$ in the CONUS by calculating the differences between drought and non-drought years (Wang et al., 2015; Borlina and Rennó, 2017; Zhao et al., 2019). Wang et al. (2015) and Zhao et al. (2019) compared the concentrations of $PM_{2.5}$ and its compositions in the southern/southeastern U.S. during the severe drought in the 2011 summertime against the non-drought year of 2010 and 2013, respectively. They show that $PM_{2.5}$ has a respective enhancement of 47% and

65% with the largest contribution from the increase of organic carbon (OC) by 119% and 117%. Following OC, sulfate in the southeast US is enhanced by 84% during the 2011 drought relative to 2013. However, fewer studies have carried out long-term analyses, which can help derive a more robust drought-aerosol association than case studies. Wang et al. (2017) performed a 25-year analysis during the growing season (March-October) from 1990 to 2014 and found that, on a monthly scale, the overall 17% enhancement of $PM_{2.5}$ in the CONUS is mainly attributed to the increase of OA, sulfate, and dust. Each of these species has a unique spatial pattern in their response to droughts, which warrants a further subregional analysis to reveal the processes causing such spatial distribution discrepancy.

In this study, we focus on the changes in OA under droughts over the CONUS during the study period of summertime from 1998 to 2018. Spatial patterns of the responses of OA to droughts will be explored, followed by a regional analysis focusing on the southeastern US (SEUS) and Pacific Northwest (PNW) where the highest responsive rates of OA to droughts are found. The processes responsible for the increase of OA in these regions will be discussed. At last, the observed drought-OA relationships will be used as a process-level metric to evaluate OA simulations in the CMIP6 ESMs, which can shed light on future model development and improve aerosol predictions.

2. Datasets

2.1 Drought indicator

The one-month gridded Standardized Precipitation-Evapotranspiration Index (SPEI) data from the global SPEI database (https://spei.csic.es/, last access: November 27, 2023) was selected as the drought indicator because of its numerical nature allowing for statistical analysis (e.g., correlation and regression). The SPEI is a multi-scaler index, allowing for the identification and comparison of drought severity through time and space (Vicente-Serrano et al., 2010). Negative values of SPEI are indicative of droughts and vice versa. The dataset has a spatial resolution of 0.5° × 0.5° and a temporal range of 1973-2018. A composite analysis can also be conducted by applying the criteria of SPEI < -1.3 and SPEI > -0.5 to denote severe drought and non-drought conditions, respectively, as suggested by Wang et al. (2017).

2.2 Air quality and meteorological data

To expand the spatial coverage, we created a gridded daily organic carbon (OC) dataset (0.5° × 0.5°) from 1998 to 2018 that aggregates site-based observations from the Interagency Monitoring of Protected Visual Environments (IMPROVE) network using the modified inverse distance weighting method as done by Schnell et al. (2014). Data from the IMPROVE sites has been widely used by previous studies to investigate surface particulate matter trends or variations in the CONUS (e.g., Hand et al., 2012). A factor of 2.1 was used to convert OC observations to OA as suggested by other studies (Pye et al., 2017; Schroder et al., 2018). US Environmental Protection Agency Chemical Speciation Network (EPA-CSN) also provides long-term OA data, but the CSN network uses different sampling practices and analytical methods from IMPROVE, which can lead to systematic differences in OA measurements

(Hand et al., 2012; Gorham et al., 2021). Thus, we only used the IMPROVE dataset in this study. To reduce the artifact caused by different data completeness (e.g., old sites retired and new sites started), we selected the sites with data records longer than 5 years during the study period for interpolation following Li and Wang (2022). Based on this criterion, there are a total of 175 sites selected for interpolation, ~80% of which have a data record equal to or greater than 15 years, suggesting small temporal uncertainties caused by the spatial interpolation (Figure S1).

Sulfate is known to influence the formation of epoxydiols derived secondary organic aerosol (IEPOX SOA), a key component of OA. To explore how this linkage changes with drought, we generated a gridded sulfate dataset following the same method as OC. Monthly sulfate wet depositions with associated precipitation amount and pH were obtained from the National Atmospheric Deposition Program (NADP). There is a total of 53 NADP sites in the SEUS (defined in Section 3.1) with a more than 5-year data record during the study period. We obtained the satellite-based low level (below 700 hPa) cloud cover and liquid water content (LWC) between 2000 to 2018 from the Clouds and the Earth's Radiant Energy System (CERES) monthly Single Scanner Footprint 1° × 1° (SSF1deg) product (https://asdc.larc.nasa.gov/project/CERES/CER_SSF1deg-Month_Terra-MODIS_Edition4A, last access: November 28, 2023). To investigate OA changes from wildfire, monthly open fire emissions were from the Global Fire Emission Database version 4 (GFED4) for 1998–2018 (Giglio et al., 2013). The version of GFED4 we used includes the burned area contributions from small fires, which increases the total amount of burned area by 75% relative to its previous version and brings the prescribed burned area estimates into closer agreement with those reported by the National Interagency Fire Center (Randerson et al., 2012). Thus, the prescribed fire burning is partly, if not all, considered in the analysis.

2.3 CMIP6 AerChemMIP models

Ten models from the CMIP6 Aerosol Chemistry Model Intercomparison Project (AerChemMIP) were selected: BCC-ESM1, CESM2-WACCM, CNRM-ESM2-1, EC-Earth3-AerChem, GFDL-ESM4, GISS-E2-1-G, MIROC6, MRI-ESM2-0, NorESM2-LM, and UKESM1-0-LL. They are the only models found by the time of writing with OA and sulfate mass concentration outputs from historical simulations with prescribed sea surface temperature in the AerChemMIP project from 1850 to 2014. No ensemble members were found for the ten models. Various aerosol schemes are used by the models with different treatments for gas phase reactions and secondary aerosol formation. More information and references (Danabasoglu et al., 2020; Dunne et al., 2020; Kelley et al., 2020; van Noije et al., 2021; Séférian et al., 2019; Seland et al., 2020; Senior et al., 2020; Tatebe et al., 2019; Wu et al., 2020; Yukimoto et al., 2019) for each model are listed in Table S1.

3. Results

3.1 Spatial Distributions of Organic Aerosol Response to Drought

Figure 1a shows the maps of the mean summertime (JJA 1998–2018) surface OA concentrations under non-drought conditions and their changes under severe droughts with the observational sites (dots) overlaid. The associated frequency and OA standard deviation during non-drought and severe drought periods are displayed in Figure S2.

The western US states along the Rocky Mountains exhibit the highest severe drought frequency of up to 25%, while wet and normal conditions are more common in the eastern US and southern California with a frequency of more than 80%. Higher OA concentrations can be found in central California and the eastern US under non-drought conditions, reflecting the average spatial distributions of summertime OA. Under severe droughts, most of the grids and sites display an enhanced OA level with a mean increase of 0.72 μg m^{-3} across all the grids and 0.78 μg m^{-3} across all the sites in the CONUS. Higher enhancements occur in the Pacific Northwest (PNW; 42-50°N, 105-125°W; red box in Figure 1a) and southeast U.S. (SEUS; 25-37°N, 75-100°W; blue box in Figure 1a). In both regions, the overall gridded OA statistical distributions under severe droughts move towards the higher end compared with those under non-drought conditions (Figure 1b), with an increase in the mean value by 1.79 μg m^{-3} (112 %) and 0.92 μg m^{-3} (33 %) across the PNW and SEUS, respectively. Similar results are found using on-site data with a respective increase of mean value by 2.18 μg m^{-3} (118 %) and 1.11 μg m^{-3} (34 %), which indicates the interpolation does not significantly affect the results. OA experienced a downward trend in the SEUS during the last two decades due to the reduction of anthropogenic emissions (Ridley et al., 2018). To verify whether the trend will significantly affect our results in the SEUS, we reproduced Figure 1b in Figure S3a using detrended OA. The detrend is conducted by removing the 7-year moving average from the raw data in the same month of each year following Wang et al. (2017) and Li et al. (2022). OA enhancement under severe droughts is 0.78 μg m^{-3} and 1.02 μg m^{-3} for gridded and on-site data, respectively, which is comparable to those values derived from raw OA data in the SEUS area. This indicates that anthropogenic emission changes do not significantly interfere with our analysis and instead natural processes play a more important role in causing the enhancement of OA in the SEUS region.

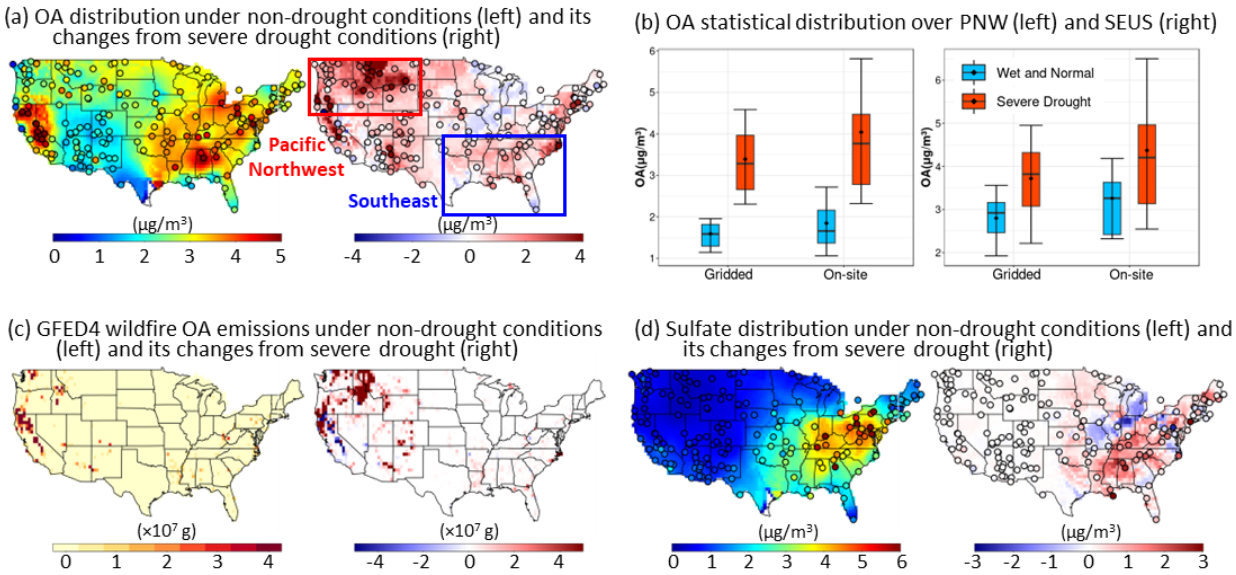

Figure 1. (a) Maps of the mean gridded and in situ (dots) OA under non-drought (wet and normal) conditions (left) from 1998 to 2018 in JJA and its changes from severe drought conditions (right). (b) Comparisons of statistical distributions of gridded and on-site OA mass concentrations under severe drought (red boxes) and non-drought (blue boxes) conditions over the Pacific Northwest (left) and southeast region (right). (c-d) Same as a, but for OA monthly wildfire emissions from GFED4 inventory and sulfate, respectively.

Wildfire, a major source of biomass burning, is one of the biggest contributors to both POA and SOA globally (Hallquist et al., 2009; Gilman et al., 2015; Jen et al., 2019). In the western U.S., OA, as the largest component of $PM_{2.5}$, experiences an upward trend, opposite to the rest of the country, due to the increasingly higher wildfire frequency (Dennison et al., 2014; McClure & Jaffe, 2018; Wang, et al., 2022). Indeed, we found many 'hot spots' of wildfire emissions of OA over the western U.S. under non-drought conditions based on the GFED4 wildfire fire inventory (Figure 1c). Severe droughts can lead to extremely high wildfire OA emissions over the PNW region, which corresponds to the highest OA enhancement and variability as shown in Figure 1a and Figure S2b, respectively. In contrast, the SEUS undergoes a much lower enhancement of wildfire OA emissions under severe droughts. Biogenic secondary organic aerosol (BSOA) is reported to be the major fine aerosol component in the SEUS, accounting for 60%–90% of the total $PM_{2.5}$, due to the abundant isoprene emissions (Zhang et al., 2012; Hidy et al., 2014; Kim et al., 2015). The concentrations of BSOA in the SEUS region strongly depend on ambient sulfate through the reactive update of gas-phase epoxydiols (IEPOX) onto the aqueous acidified surface of sulfate particles (Surratt et al., 2010; Xu et al., 2015; Lopez-Hilfiker et al., 2016; Malm et al., 2017). Interestingly, the highest sulfate increase during drought is found in the SEUS (Figure 1d), presumably due to enhanced gas-phase sulfate production and reduced wet deposition (Wang et al., 2015; Xie et al., 2019). The higher sulfate concentrations during droughts lead to the enhanced formation of IEPOX SOA, which is likely an important factor leading to a higher OA level in the SEUS.

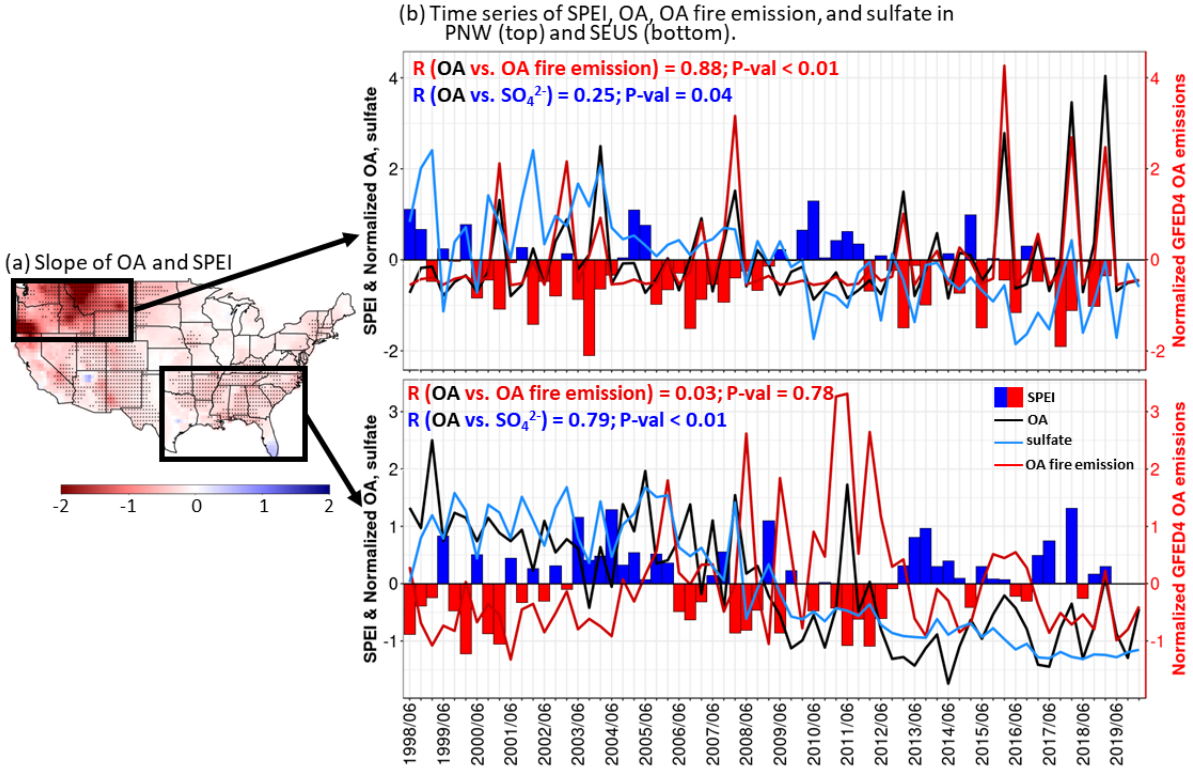

Figure 2. (a) Map of the slopes between monthly gridded OA and SPEI. Black dots indicate the slopes with P-vales less than 0.05. (b) Time series of SPEI (bar), normalized OA (black line), sulfate (blue line), and wildfire OA emissions from GFED4 inventory (red line; right axis) averaged across the PNW (top) and SEUS (bottom) region. The numbers indicate the correlation coefficient (R) and P-value (P-val) between OA and sulfate (blue) and wildfire emissions (red).

Using the numerical drought indicator of SPEI, we calculated the linear slopes between monthly OA and SPEI in each grid (Figure 2a). Consistent with the composite analysis in Figure 1a, most of the grids show negative slopes with the highest absolute values of more than 2 $\mu g\ m^{-3}$ per unit change of SPEI occurring in the PNW region. It is noteworthy that negative values of SPEI indicate droughts, and thus the negative slopes with SPEI signify an enhanced OA level over most of the CONUS during drought. We further examined the monthly time series of the regional mean of SPEI, normalized OA, sulfate, and OA wildfire emissions in the PNW and SEUS (Figure 2b). OA in the PNW region is strongly correlated with OA emissions from fire with a high correlation coefficient (R) of 0.88. The extremely high values of OA and OA fire emissions are also concurrent with droughts when SPEI is negative (red bars). On the contrary, SEUS has a weak correlation between OA and OA fire emissions yet a high association between OA and sulfate with an R value of 0.79. Wildfire seems only to have high contributions to peak OA values in extreme drought years, such as in 2011. Based on the correlation coefficients, more than 60% and 70% of the monthly OA variability can be explained by sulfate and wildfire emissions in the SEUS and PNW regions, respectively, which deserves an in-depth exploration in the next section.

3.2 Regional Analysis in the Pacific Northwest and Southeast US

In this section, we conducted a regional analysis of OA, focusing on OA relationships with sulfate in the SEUS and with wildfire emissions in the PNW. In the SEUS, we calculated the linear regression between OA and sulfate in Figure 3a following the method of Malm et al. (2017). Each data point represents the SPEI bin-averaged value of OA and sulfate from each grid cell. The bins are divided to have approximately the same number of samples following Xie et al (2019). Only the grids with all five SPEI bins present are used (N=673), which include more than 95% of the total grids (687). Thus, the binned regression calculation can represent the regional conditions of each SPEI bin. The resulting linear lines and formula are also displayed in Figure 3a. Here the slope calculation is different from Zheng et al. (2020), in which they averaged OA and sulfate across all the sites in the SEUS and performed the linear regression temporally. We adopted a spatial calculation of the linear slopes for two reasons: (1) Averaging across all the sites/grids will significantly reduce the number of data points after the allocation among SPEI bins; (2) The regional mean of SPEI may average out some drought signals because drought is grid specific and can differ spatially within the SEUS (Ford et al., 2014). Despite the different methods used, the linear slope in our calculation (0.56) under non-drought conditions is similar to that of Zheng et al. (2020) using SEARCH (SouthEastern Aerosol Research and Characterization) sites (0.51). Therefore, our linear slope calculation method reproduces the sensitivity of OA to sulfate reported by the existing studies.

As SPEI changes from positive (non-drought) to negative (drought), the slope between OA and sulfate becomes increasingly higher, ranging from 0.56 to 0.79. This indicates more OA formations per unit increase in sulfate as drought severity intensifies. Although high correlations do not necessarily indicate causal relationships, the chemical

mechanism of IEPOX SOA formation with the presence of sulfate is well documented (e.g., Shrivastava et al., 2017). The higher sensitivities of OA to sulfate under droughts can be explained by the increasingly higher isoprene concentrations as shown in our previous studies in the SEUS (Li et al., 2022; Wang et al., 2022b), resulting in more IEPOX in the atmosphere to be further converted to particle phase catalyzed by sulfate. In addition, the formation of monoterpene-derived organosulfates, a major component of IEPOX SOA, is also dependent on sulfate (D'Ambro et al., 2019) and the biogenic emissions of monoterpenes are likely to be intensified during droughts (Llusià et al., 2008; Wu et al., 2015). Organosulfates originated from anthropogenic precursors are also reported by some studies (Riva et al., 2015; Le Breton et al., 2018), but they are mainly found in highly polluted urban areas. We further reproduced Figure 3a using detrended OA and sulfate data, which can remove the effects of anthropogenic emissions (Figure S3b). A similar pattern of the gradually increasing slope from the wettest (slope=0.18) to the driest (slope=0.48) SPEI bin was found, which verifies the stronger dependence of OA on sulfate under droughts is mainly caused by biogenic sources.

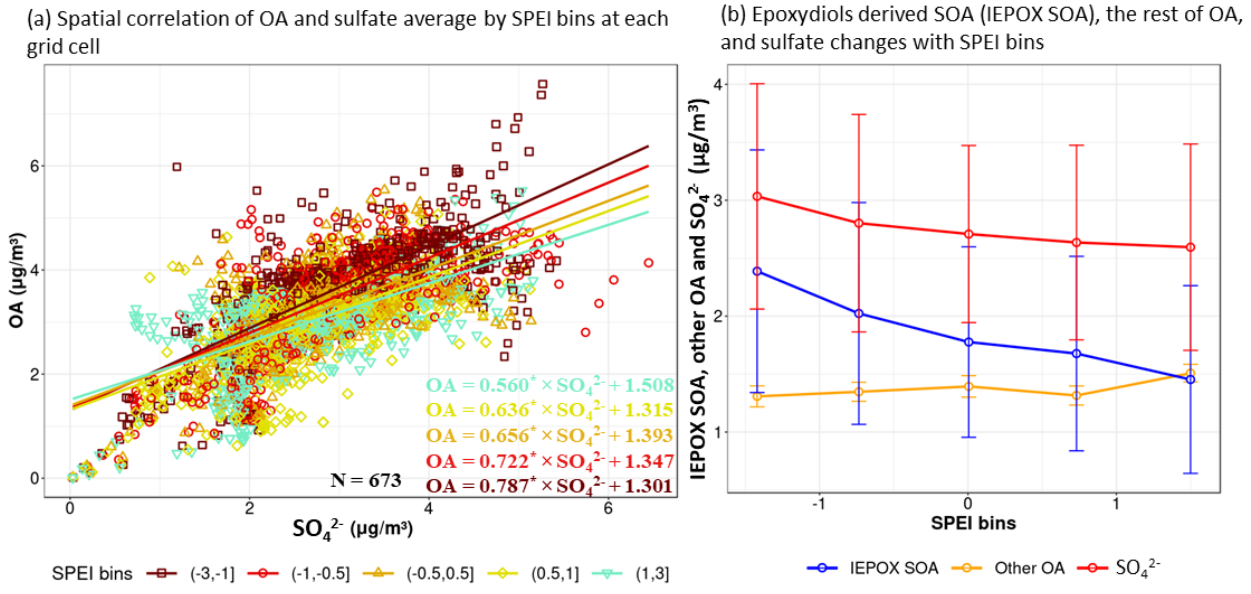

Figure 3. (a) Scatter plot of the SPEI bin-averaged sulfate and OA at each grid in the SEUS with solid lines representing the linear regressions of OA and sulfate. The corresponding linear formula of each SPEI bin is listed in the bottom-right corner with N indicating the number of data points for each regression calculation. The star marks in the formula indicate the regression significance at a 95% confidence level. (b) The epoxydiols derived SOA (IEPOX SOA), other SOA, and sulfate changes with SPEI derived from the linear regressions in a. Vertical bars indicate one standard deviation.

The intercept of the linear regression can be interpreted as other OA components that are not associated with sulfate-catalyzed IEPOX SOA, such as POA and anthropogenic SOA (Malm et al., 2017). Figure 3b shows that the intercepts (other OA) are stable among the five SPEI bins with a less than 0.2 μg m^{-3} (15%) difference. The differences of regional mean OA minus the intercepts can then be considered as IEPOX SOA related to sulfate. The resulting estimate of IEPOX SOA is 1.45 μg m^{-3}, 1.68 μg m^{-3}, 1.78 μg m^{-3}, 2.02 μg m^{-3} and 2.39 μg m^{-3} for the five SPEI bins ranging from wet to dry conditions. These values correspond to an increase of 0.30 μg m^{-3} IEPOX SOA

per unit decrease in SPEI. Interestingly, there is also an increasingly higher sulfate level from wet to dry SPEI bins with a mean value of 2.59 μg m^{-3}, 2.63 μg m^{-3}, 2.71 μg m^{-3}, 2.80 μg m^{-3} and 3.03 μg m^{-3}, respectively, corresponding to an overall increase rate of 0.14 μg m^{-3} sulfate per unit decrease of SPEI. Therefore, the increase of OA in the SEUS under droughts is largely caused by the boosted formation of BSOA due to the concurrent increase in VOC emissions and sulfate. This is consistent with the modeling case study by Zhao et al. (2019) who found that 98% of the SOA increase during drought in the SEUS is of biogenic origin. It is noted that the approximation of IEPOX SOA here is the upper limit of BSOA since other processes that can lead to the simultaneous changes of sulfate and OA, such as wildfire, are miscounted as BSOA in the calculation. Further analysis is needed to attribute the changes of SOA to different sources more accurately.

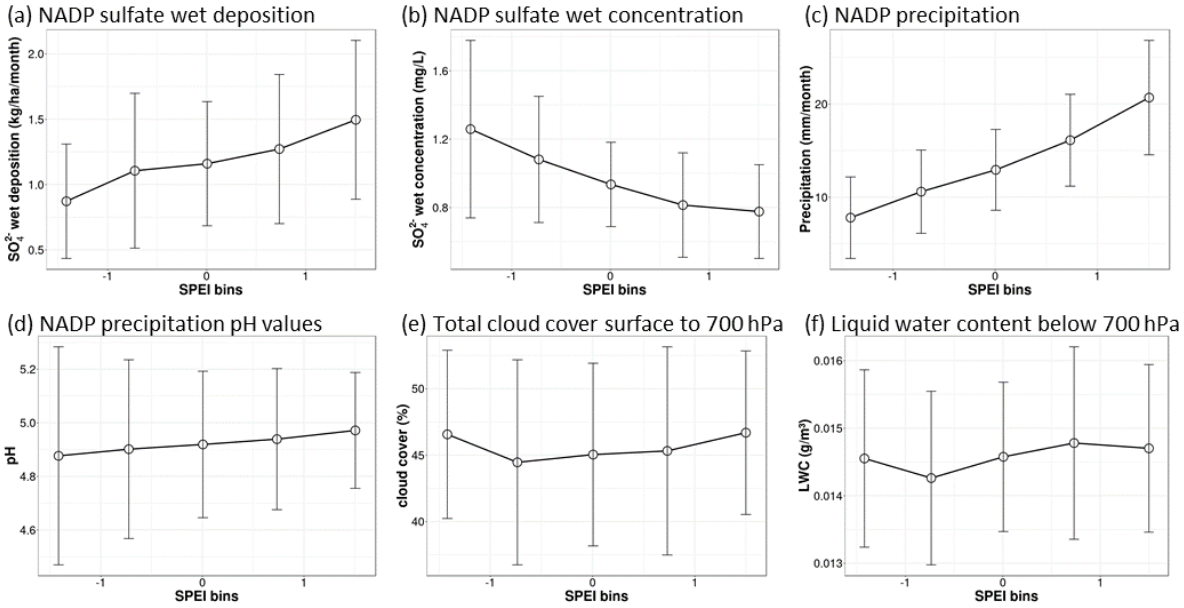

Figure 4. SPEI bin-averaged sulfate wet deposition (a), wet concentration (b), precipitation amount (c), precipitation pH values (d) from the NADP network, and the total cloud cover (e) and liquid water content (LWC; f) below 700 hPa from the MODIS satellite in the SEUS. Vertical bars indicate one standard deviation.

The source and sink of atmospheric sulfate are greatly affected by clouds and precipitation because most of the sulfate is formed in clouds and efficiently removed by wet scavenging (Barth et al., 2000; Rasch et al., 2000; Berg et al., 2015). Thus, it is understandable that sulfate is sensitive to drought considering both clouds and precipitation are significantly modulated under droughts. To further investigate the processes causing the increase of sulfate, we analyzed sulfate wet deposition, wet concentration, precipitation amount, and pH values (Figure 4a-d) from the NADP network. There is a decreasing trend of sulfate wet deposition from 1.50 kg ha^{-1} $month^{-1}$ at the wettest (SPEI > 1) to 0.87 kg ha^{-1} $month^{-1}$ at the driest (SPEI < -1) level. The corresponding reduction in precipitation is 62%. Since sulfate wet deposition is calculated using sulfate wet concentration weighted by precipitation, the 50% decrease of sulfate wet deposition is driven by the reduced precipitation, which outweighs the increase of sulfate concentrations.

The low level (below 700 hPa) cloud cover and liquid water content (LWC) are not highly sensitive to droughts with less than 2% and 4% changes among the five SPEI bins, respectively (Figure 4e-f). Thus, the increase of sulfate wet concentrations in precipitation is likely indicative of an enhanced formation of aqueous sulfate in the clouds, which then precipitates. Alternatively, gas phase production of sulfate can also be elevated under droughts due to more sulfur dioxide (SO_2) emissions (e.g. from increased electricity generation and fires) and higher temperatures (Tai et al., 2010; Wang et al., 2017), and then washed out by rainwater droplets causing higher sulfate wet concentrations in precipitation. Either of these two pathways suggests that there is higher sulfate formation under droughts which contributes to the enhanced sulfate besides reduced wet deposition. Furthermore, the mean pH value drops steadily with dryness levels from 4.98 to 4.87, which further intensifies the acid-catalyzed IEPOX ring opening and leads to faster BSOA formation (Surratt et al., 2010). Although the rate of IEPOX SOA formation is slower in cloud water compared to aerosol particles due to its relatively higher pH values (Gaston et al., 2014), the large liquid water content of clouds, which promotes dissolution, could lead to significant IEPOX SOA formation. Based on a box model simulation conducted by Tsui et al (2019), increasing pH values in cloud water while keeping the other factors constant results in a slower rate of IEPOX SOA formation. Additionally, cloud water processing at $pH \leq 4$ can produce more IEPOX SOA than aerosol particles. Despite the average pH value of ~5 across the SEUS region, some sites may experience more acidic rainwater in drought months. During the study period, we found two sites in Georgia and North Carolina with pH less than 4 and their corresponding SPEI values are –0.98 and –1.39. Therefore, droughts are likely to reduce cloud pH values lower enough at some locations and favorable for significant IEPOX SOA formation.

Using the same approach as in the SEUS, we calculated the SPEI bin-averaged OA and OA wildfire emissions from the GFED4 inventory in the PNW region shown in Figure 5. OA fire emissions grow from 0.09×10^7 g per month at the wettest level to 4.94×10^7 g per month at the second driest level (SPEI between -1.5 and -1), followed by a small drop to 4.17×10^7 g per month at the driest level (SPEI less than -1.5). This drop is likely caused by the reduction in the supply of fire fuel load under extreme drought conditions (Scasta et al., 2016). Overall, OA fire emissions increase by 1.44×10^7 g per unit decrease of SPEI per month. The mass concentrations of OA resemble the changes of OA fire emissions with an overall increase rate of 1.01 μg m^{-3} per unit decrease of SPEI, which indicates more wildfire emissions are the major driver of the higher OA concentrations in the PNW.

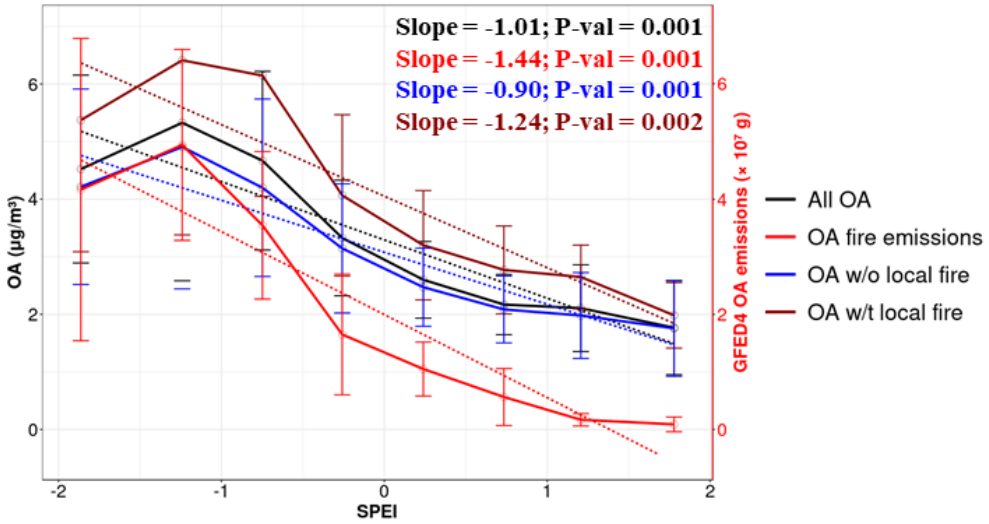

Figure 5. Mean (point) and one standard deviation (vertical bar) of OA (black line), wildfire OA emissions from GFED4 inventory (bright red line; right axis), and OA with (dark red line) and without (blue line) local fire occurrence within each SPEI bin. The dashed lines represent the linear regression with the slopes (Slope) and P-values (P-val) of each variable listed in the top-right corner.

To better quantify the contributions of wildfire, we further separated OA values into those with local fire influences if OA fire emissions are greater than zero at each grid in each month and those without local fire influences if zero fire emissions are found. The time series of OA grouped by periods with and without wildfire emissions within each SPEI bin (Figure S4) shows that the two groups have nearly identical temporal coverage with data found in almost all years within most SPEI bins, which indicates the separation does not cause temporal inconsistency. We admit that this separation relies on the accuracy of fire emissions and cannot rule out the effects of the long-range transported OA from other regions, especially for the widespread drought events. As a result, it may overestimate OA values with no local fire occurrence. With this caveat in mind, we calculated the local fire effects as the difference between OA with and without fire emissions within each drought bin. Under the wettest conditions, there is a minor difference of 0.23 $\mu g\ m^{-3}$ between OA with and without local fire effects, while this number becomes four to eight times higher under droughts (SPEI < zero). The local fire-affected OA with one unit decrease of SPEI also increases by 0.34 $\mu g\ m^{-3}$ faster than that without local fire occurrence. This illustrates the considerable contributions of local wildfire emissions to the changes of OA under droughts. Other processes, such as long-range transported aged OA and locally produced BSOA, may also contribute to the differences if their contributions correlate with local fire emissions.

In summary, there is an increasing sensitivity of OA to sulfate as drought conditions worsen in the SEUS, driven by the heightened biogenic VOC emissions and the subsequent formation of IEPOX SOA. Sulfate levels also rise under droughts, influenced mainly by the reduced precipitation and the potentially increased aqueous and gas-phase sulfate production. In the PNW, OA and OA wildfire emissions exhibit a close correlation, indicating that wildfire emissions significantly drive higher OA concentrations therein.

3.3 CMIP6 Models Simulated Organic Aerosol Response to Drought

In this section, we evaluated the surface OA concentrations from ten CMPI6 models regarding their capability in predicting the observed SPEI-OA relationships over the CONUS during JJA 1998-2014. OA values from each model were interpolated linearly to match the spatial resolution of the gridded observational dataset. Figure 6a-j show the spatial distributions of the slopes between SPEI and OA simulated by each model. Compared with the observed slopes in Figure 2a, all models capture the strong negative slopes of more than 2 $\mu g\, m^{-3}$ per unit decrease of SPEI in the PNW region except for GFDL-ESM4 which shows a much smaller slope of less than 1 $\mu g\, m^{-3}$ per SPEI. This indicates the CMIP6 models correctly represent the sign and magnitude of the changes in OA fire emissions with droughts. By contrast, all the models have difficulties in reproducing the observed linear relationships between OA and SPEI in the SEUS. Compared to the significantly negative slope from observations, most of the models display insignificant or even positive slopes in the SEUS. BCC-ESM1, MRI-ESM2-0, and Nor-ESM2-LM show negative slopes only in part of the SEUS grids.

We also evaluated model predicted average OA enhancement under server droughts relative to non-drought periods in PNW and SEUS (Figure 6k). In the PNW region, CESM2-WACCM simulates an increase of OA mass concentration by 2.20 $\mu g\, m^{-3}$, closest to the observed value of 2.41 $\mu g\, m^{-3}$, followed by UKESM1-0-LL and CNRM-ESM2-1 with an enhancement of 1.74 $\mu g\, m^{-3}$ and 1.64 $\mu g\, m^{-3}$, respectively. GFDL-ESM4 shows the highest underestimation of the OA enhancement by 2 $\mu g\, m^{-3}$ (83%), consistent with its smallest slopes shown in Figure 6e. Smaller underestimations are found in other models, ranging from 0.96 $\mu g\, m^{-3}$ (40%) for MRI-ESM2-0 to 1.4 $\mu g\, m^{-3}$ (58%) for EC-Earth3-AerChem. In the SEUS, all the ten models underpredict the observed OA increase of 0.57 $\mu g\, m^{-3}$ with the two lowest underestimations of 0.21 $\mu g\, m^{-3}$ (37%) and 0.27 $\mu g\, m^{-3}$ (47%) found for Nor-ESM2-LM and MIRCO6, respectively. The other eight models show marginal OA enhancements between 0.02 $\mu g\, m^{-3}$ to 0.21 $\mu g\, m^{-3}$ or even a decrease (GISS-E2-1-G), indicating the incapabilities of these models in predicting OA changes in the SEUS under droughts.

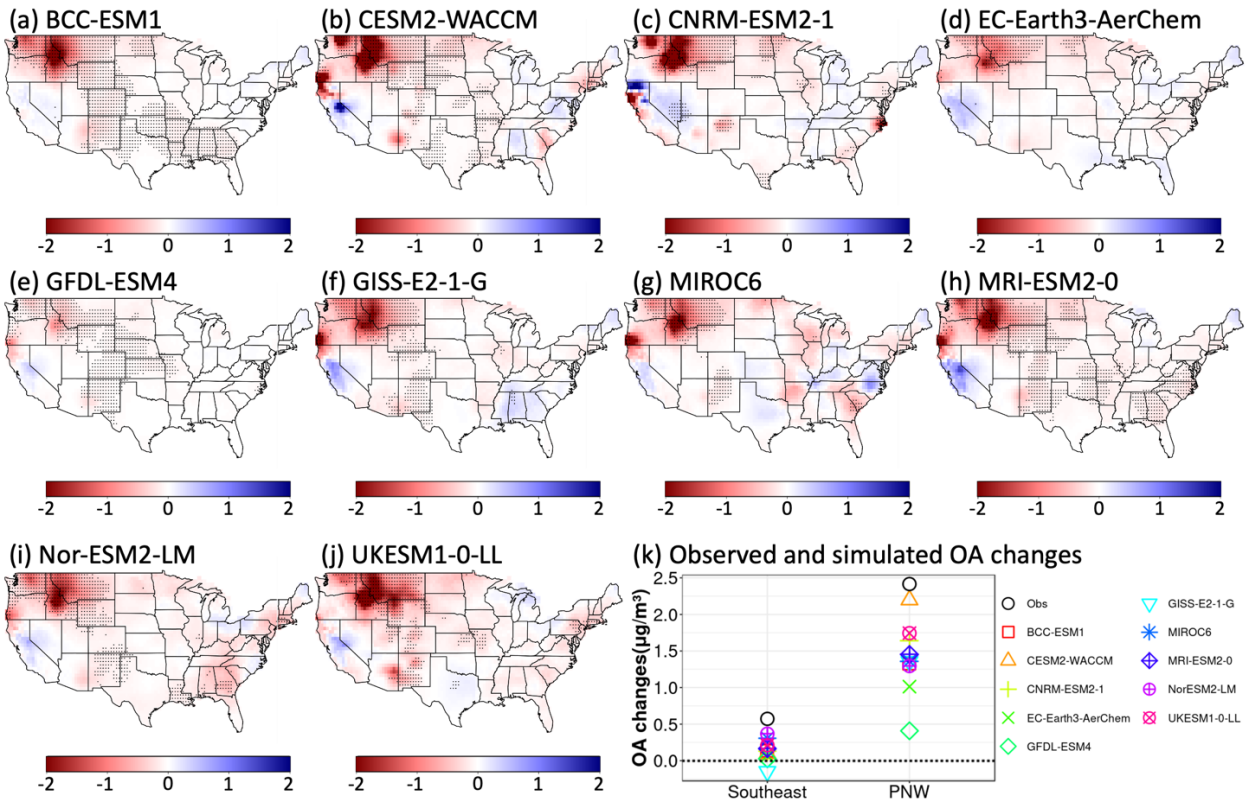

Figure 6. (a-j) Slopes between CMIP6 model simulated OA and SPEI from 1998 to 2014 during summertime with black dots indicating the P-values less than 0.05. (k) Observed and simulated OA changes under severe droughts relative to non-drought conditions during the same study period in the PNW and SEUS regions.

The poor model performance in capturing the OA changes under severe drought in the SEUS inspires us to conduct a further regional analysis following Section 3.2. The observed and simulated changes of SEUS-mean OA, sulfate, and their slopes within each SPEI bin are shown in Figure 7a-c, respectively. The modeled slopes are calculated in the same way as observations (Figure 3a) and the associated scatter plot is shown in Figure S5. For the absolute OA mass concentrations, UKESM1-0-LL has the best predictions with a less than 0.5 μg m^{-3} mean bias in each SPEI bin. CESM2-WACCM, CNRM-ESM2-1, EC-Earth3-AerChem, MICRO6, and NorESM2-LM overestimate OA values, while the other four models show an underestimation. For the sensitivity of OA to droughts, NorESM2-LM performs the best with an increase rate of 0.13 μg m^{-3} per unit decrease of SPEI, although the rate is only 50% of the observed value of 0.25 μg m^{-3}. This is consistent with the result that this model has the lowest underestimation of OA enhancement under severe droughts. Higher underestimations of the OA sensitivity to droughts are found in MRI-ESM2-0, BCC-ESM1, and GFDL-ESM4 with a respective change rate of 0.09 μg m^{-3}, 0.06 μg m^{-3} and 0.02 μg m^{-3} per SPEI. On the contrary, GISS-E2-1-G simulates a decrease in OA by 0.04 μg m^{-3} per unit decrease of SPEI, which is consistent with the negative OA changes under severe droughts. The rest of the models do not have a statistically significant change rate of OA with droughts at a 95% confidence level.

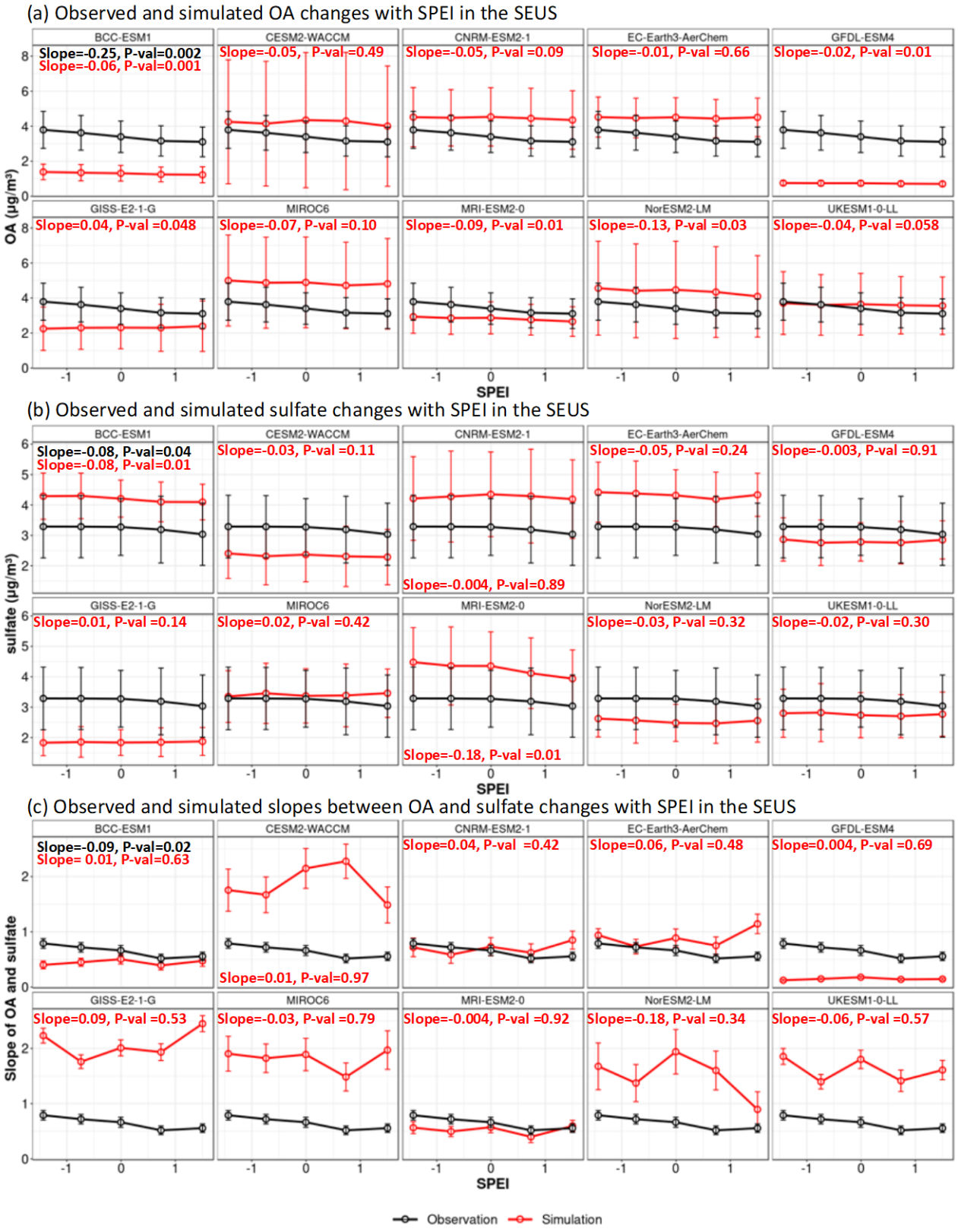

Figure 7. SPEI bin-averaged values of OA (a), sulfate (b), and slopes of OA and sulfate (c) from observations (black lines) and simulations (red lines) in the SEUS. Vertical bars indicate one standard deviation. The numbers in each subplot indicate the slopes (Slope) and P-values (P-val) of the linear regression between each variable and SPEI.

As described in Figure 3, the increase of OA under droughts in the SEUS is due to the concurrent increase of sulfate and biogenic VOC emissions. To investigate if the models have this mechanism, we also evaluated the modeled sensitivities of sulfate and the OA-sulfate slopes to SPEI. Only two models, BCC-ESM1 and MRI-ESM2-0, have statistically significant increase rates of sulfate with the decrease of SPEI, despite their overestimation of ~1 $\mu g\ m^{-3}$ (30%) in terms of the absolute sulfate concentrations. BCC-ESM1 predicts the same change rate as observations with a value of 0.08 $\mu g\ m^{-3}$ per unit change of SPEI, while MRI-ESM2-0 predicts a rate of 0.18 $\mu g\ m^{-3}$, more than doubled the observed rate. For the slopes between OA and sulfate, however, all models cannot reproduce the observed increase rate of 0.09 per unit decrease of SPEI. This suggests either an insensitivity of biogenic VOC emissions in response to droughts or a lack of explicit aqueous chemistry for SOA formation in the models. For a further investigation, we summarized how SOA is treated in each model (Table S1). In fact, SOA schemes in the 10 CMIP6 models are simplified to reduce computational cost as the climate models need to perform hundreds of years of simulations with many ensemble members (Eyring et al., 2016). BCC-ESM1 and CESM2-WACCM use a volatility basis set (VBS) approach that categorizes VOCs based on their volatility and simulates the chemical aging process that leads to the formation of SOA. In CNRM-ESM2-1, SOA is prescribed from a monthly inventory without inline calculation. EC-Earth3-AerChem, GISS-E2-1-G, and MIROC6 include the two-product scheme, in which VOC oxidation leads to non-volatile and semi-volatile products. The rest of the models assume a fixed percentage of yield from the emissions of VOCs. In short, the heterogeneous formation of IEPOX SOA through reactive uptake on aqueous sulfate is not parameterized in the models. Therefore, the linear relationship between OA and sulfate in the models is not indicative of the mechanistic dependence of OA on sulfate as demonstrated in observations. Similar anthropogenic sources (e.g., fossil fuel combustion) and photochemical oxidants (e.g., O3 and OH) leading to the simultaneous production of sulfate and OA can also result in positive correlations (Zhang et al., 2011). The lack of the IEPOX SOA formation mechanism further explains why the enhancements of OA in the SEUS are barely captured by these models. To sum up, most of the models can represent the linear relationships between OA and SPEI in the PNW region with CESM2-WACCM and GFDL-ESM4 performing the best and worst in predicting the OA enhancement under severe droughts. However, all the models face challenges in capturing the OA increases under droughts in the SEUS, with Nor-ESM2-LM and MIRCO6 showing relatively better performance indicated by their lower underestimation of OA enhancement. These challenges are mainly caused by the lack of parameterizations of the aqueous formation of IEPOX SOA and the model deficiencies in capturing the increase pattern of sulfate as drought intensifies.

4 Conclusions

In this study, the changes in organic aerosol (OA) in response to drought in the CONUS were examined. We first displayed the spatial patterns of OA under non-drought and severe drought conditions and found most of the CONUS experiences an abnormally higher level of OA by an average of 0.72 $\mu g\ m^{-3}$ relative to wet and normal conditions. Regionally, the highest average increase occurs in the PNW and SEUS areas by 1.79 $\mu g\ m^{-3}$ (112 %) and

0.92 μg m^{-3} (33 %), respectively. The concurrent enhancement of wildfire OA emissions in the PNW and sulfate in the SEUS provides more insights into an in-depth investigation over these two regions.

In the SEUS, a linear regression between OA and sulfate was applied to estimate the amount of IEPOX SOA and other OA. Although a similar method has also been used by other studies (e.g., Malm et al., 2017), it is necessary to be aware of its limitations that the approximation of IEPOX SOA is the upper limit of BSOA since other processes that can lead to the simultaneous changes of sulfate and OA are miscounted as BSOA in the calculation. Results from this simplified method indicate that the IEPOX SOA drives the increase of total OA from wet to dry conditions while other OA stays stable. Both the increase of biogenic VOC emissions and sulfate under droughts lead to the enhancement of IEPOX SOA. Data from the NADP network shows that up to 62% lower precipitation under droughts induces slower sulfate wet deposition rates and thus leaves more sulfate in the atmosphere. Higher sulfate wet concentration in the precipitation indicates more in-cloud and/or gas-phase sulfate production under droughts since cloud cover and liquid content do not show a strong sensitivity to droughts.

In the PNW, there is an overall increase of 1.44×10^7 g in the monthly OA wildfire emissions per unit decrease of SPEI, which is the main driver of the elevated OA. There is a plateau of the OA fire emissions with SPEI between -1.5 and -1, followed by a drop with SPEI less than -1.5. This implies that wildfire activities are not linearly related to moisture and are also limited by the availability of fuel load. Dividing OA into groups with or without local fire influence, we found that local fire events can increase the OA concentrations by four to eight times relative to those without fire activities. Future work is needed to further investigate the changes in OA from other sources, such as long-range transported OA and BSOA, in this region.

The evaluation of surface OA concentrations from ten CMIP6 models provides valuable insights into their predictive capabilities in capturing the observed relationships between SPEI and OA over the CONUS. All the models are found to successfully capture the negative slopes in the PNW area, indicating correct sensitivities of OA wildfire emissions to droughts in these models. However, deficiencies are revealed in the SEUS with most models displaying insignificant or positive slopes between OA and SPEI as opposed to significantly negative slopes from observations. The assessment of average OA enhancement during severe droughts relative to non-drought periods further underscores the models' varying degrees of accuracy in simulating OA response to drought. In the PNW, CESM2-WACCM stands out with its simulated OA increase of 2.20 μg m^{-3} being closest to the observed value of 2.41 μg m^{-3}, while GFDL-ESM4 exhibits the highest underestimation of OA enhancement by 2 μg m^{-3} (83%). In the SEUS, all models consistently underpredict the observed OA increases, highlighting their limitations in predicting OA changes in this region under drought conditions. These limitations can be mainly attributed to the insensitivities of sulfate to SPEI and the model deficiencies in the parameterization of the IEPOX SOA dependence on inorganic sulfate.

This study reveals the key drivers of the enhanced OA mass concentrations in the CONUS, including higher wildfire emissions and the simultaneous increase in biogenic VOC emissions and inorganic sulfate, which highlights the complex physical and chemical processes involved in the aerosol composition changes under droughts. The

discrepancies in simulating OA enhancements during severe droughts underscore the need for ongoing model improvement, particularly in accurately representing the emissions of biogenic isoprene and monoterpene, the life cycle of sulfate, and their intricate interactions. Addressing these limitations will be crucial for enhancing the reliability of climate models and their ability to predict the impact of future droughts on atmospheric composition and air quality in the CONUS.

Data availability

Monthly SPEI data is obtained from https://spei.csic.es/spei_database_2_6 (Vicente-Serrano et al., 2010). Observations from the IMPROVE and NADP network are downloaded from https://views.cira.colostate.edu/fed/QueryWizard/ (FED, 2023). GFED4 wildfire emission inventory and MODIS satellite cloud cover data are archived at https://www.geo.vu.nl/~gwerf/GFED/GFED4/ (Giglio et al., 2013) and https://asdc.larc.nasa.gov/project/CERES/CER_SSF1deg-Month_Terra-MODIS_Edition4A (NASA, 2015), respectively. The CMIP6 model outputs are publicly available online from the Earth System Federation Grid nodes.

Competing interests

The authors declare that they have no conflict of interest.

Author contributions

YW conceived the research idea. WL conducted the analysis. Both authors contributed to the preparation of the manuscript.

Acknowledgments

The authors acknowledge researchers from the IMPROVE and NADP networks for making surface aerosol mass and deposition observations. We thank individuals and groups from the Climatology and Climate Services Laboratory for creating the SPEI dataset. The authors also thank the modeling groups participating in the CMIP6 AerChemMIP project for making the surface aerosol species outputs available.

Financial support

This research has been supported by the National Oceanic and Atmospheric Administration through the Atmospheric Chemistry, Carbon Cycle and Climate (AC4) Program (grant no. NA19OAR4310177).

References

Barth, M. C., Rasch, P. J., Kiehl, J. T., Benkovitz, C. M., and Schwartz, S. E.: Sulfur chemistry in the National Center for Atmospheric Research Community Climate Model: Description, evaluation, features, and sensitivity to aqueous chemistry, J. Geophys. Res. Atmospheres, 105, 1387–1415, https://doi.org/10.1029/1999JD900773, 2000.

Berg, L. K., Shrivastava, M., Easter, R. C., Fast, J. D., Chapman, E. G., Liu, Y., and Ferrare, R. A.: A new WRF-Chem treatment for studying regional-scale impacts of cloud processes on aerosol and trace gases in parameterized cumuli, Geosci. Model Dev., 8, 409–429, https://doi.org/10.5194/gmd-8-409-2015, 2015.

Borlina, C. S. and Rennó, N. O.: The impact of a severe drought on dust lifting in California's Owens Lake area, Sci. Rep., 7, 1784, https://doi.org/10.1038/s41598-017-01829-7, 2017.

Brégonzio-Rozier, L., Giorio, C., Siekmann, F., Pangui, E., Morales, S. B., Temime-Roussel, B., Gratien, A., Michoud, V., Cazaunau, M., DeWitt, H. L., Tapparo, A., Monod, A., and Doussin, J.-F.: Secondary organic aerosol formation from isoprene photooxidation during cloud condensation–evaporation cycles, Atmospheric Chem. Phys., 16, 1747–1760, https://doi.org/10.5194/acp-16-1747-2016, 2016.

Brilli, F., Barta, C., Fortunati, A., Lerdau, M., Loreto, F., and Centritto, M.: Response of isoprene emission and carbon metabolism to drought in white poplar (Populus alba) saplings, New Phytol., 175, 244–254, https://doi.org/10.1111/j.1469-8137.2007.02094.x, 2007.

Carslaw, K. S., Lee, L. A., Reddington, C. L., Pringle, K. J., Rap, A., Forster, P. M., Mann, G. W., Spracklen, D. V., Woodhouse, M. T., Regayre, L. A., and Pierce, J. R.: Large contribution of natural aerosols to uncertainty in indirect forcing, Nature, 503, 67–71, https://doi.org/10.1038/nature12674, 2013.

Cook, B. I., Mankin, J. S., and Anchukaitis, K. J.: Climate change and drought: From past to future, Curr. Clim. Change Rep., 4, 164–179, https://doi.org/10.1007/s40641-018-0093-2, 2018.

D'Ambro, E. L., Schobesberger, S., Gaston, C. J., Lopez-Hilfiker, F. D., Lee, B. H., Liu, J., Zelenyuk, A., Bell, D., Cappa, C. D., Helgestad, T., Li, Z., Guenther, A., Wang, J., Wise, M., Caylor, R., Surratt, J. D., Riedel, T., Hyttinen, N., Salo, V.-T., Hasan, G., Kurtén, T., Shilling, J. E., and Thornton, J. A.: Chamber-based insights into the factors controlling epoxydiol (IEPOX) secondary organic aerosol (SOA) yield, composition, and volatility, Atmospheric Chem. Phys., 19, 11253–11265, https://doi.org/10.5194/acp-19-11253-2019, 2019.

Danabasoglu, G., Lamarque, J.-F., Bacmeister, J., Bailey, D. A., DuVivier, A. K., Edwards, J., Emmons, L. K., Fasullo, J., Garcia, R., Gettelman, A., Hannay, C., Holland, M. M., Large, W. G., Lauritzen, P. H., Lawrence, D. M., Lenaerts, J. T. M., Lindsay, K., Lipscomb, W. H., Mills, M. J., Neale, R., Oleson, K. W., Otto-Bliesner, B., Phillips, A. S., Sacks, W., Tilmes, S., van Kampenhout, L., Vertenstein, M., Bertini, A., Dennis, J., Deser, C., Fischer, C., Fox-Kemper, B., Kay, J. E., Kinnison, D., Kushner, P. J., Larson, V. E., Long, M. C., Mickelson, S., Moore, J. K., Nienhouse, E., Polvani, L., Rasch, P. J., and Strand, W. G.: The Community Earth System Model Version 2 (CESM2), J. Adv. Model. Earth Syst., 12, e2019MS001916, https://doi.org/10.1029/2019MS001916, 2020.

Dawson, J. P., Adams, P. J., and Pandis, S. N.: Sensitivity of $PM_{2.5}$ to climate in the Eastern US: a modeling case study, Atmospheric Chem. Phys., 7, 4295–4309, https://doi.org/10.5194/acp-7-4295-2007, 2007.

Dennison, P. E., Brewer, S. C., Arnold, J. D., and Moritz, M. A.: Large wildfire trends in the western United States, 1984–2011, Geophys. Res. Lett., 41, 2928–2933, https://doi.org/10.1002/2014GL059576, 2014.

Dunne, J. P., Horowitz, L. W., Adcroft, A. J., Ginoux, P., Held, I. M., John, J. G., Krasting, J. P., Malyshev, S., Naik, V., Paulot, F., Shevliakova, E., Stock, C. A., Zadeh, N., Balaji, V., Blanton, C., Dunne, K. A., Dupuis, C., Durachta, J., Dussin, R., Gauthier, P. P. G., Griffies, S. M., Guo, H., Hallberg, R. W., Harrison, M., He, J., Hurlin, W., McHugh, C., Menzel, R., Milly, P. C. D., Nikonov, S., Paynter, D. J., Ploshay, J., Radhakrishnan, A., Rand, K., Reichl, B. G., Robinson, T., Schwarzkopf, D. M., Sentman, L. T., Underwood, S., Vahlenkamp, H., Winton, M., Wittenberg, A. T., Wyman, B., Zeng, Y., and Zhao, M.: The GFDL Earth System Model Version 4.1 (GFDL-ESM 4.1): Overall Coupled Model Description and Simulation Characteristics, J. Adv. Model. Earth Syst., 12, e2019MS002015, https://doi.org/10.1029/2019MS002015, 2020.

Eyring, V., Bony, S., Meehl, G. A., Senior, C. A., Stevens, B., Stouffer, R. J., and Taylor, K. E.: Overview of the Coupled Model Intercomparison Project Phase 6 (CMIP6) experimental design and organization, Geosci. Model Dev., 9, 1937–1958, https://doi.org/10.5194/gmd-9-1937-2016, 2016.

Fang, Y., Fiore, A. M., Horowitz, L. W., Gnanadesikan, A., Held, I., Chen, G., Vecchi, G., and Levy, H.: The impacts of changing transport and precipitation on pollutant distributions in a future climate, J. Geophys. Res. Atmospheres, 116, https://doi.org/10.1029/2011JD015642, 2011.

FED: The Federal Land Manager Environmental Database query wizard, FED, https://views.cira.colostate.edu/fed/QueryWizard/ (last access: 27 December 2023), 2023.

Gaston, C. J., Riedel, T. P., Zhang, Z., Gold, A., Surratt, J. D., and Thornton, J. A.: Reactive Uptake of an Isoprene-Derived Epoxydiol to Submicron Aerosol Particles, Environ. Sci. Technol., 48, 11178–11186, https://doi.org/10.1021/es5034266, 2014.

Giglio, L., Randerson, J. T., and van der Werf, G. R.: Analysis of daily, monthly, and annual burned area using the fourth-generation global fire emissions database (GFED4), J. Geophys. Res. Biogeosciences, 118, 317–328, https://doi.org/10.1002/jgrg.20042, 2013.

Gilman, J. B., Lerner, B. M., Kuster, W. C., Goldan, P. D., Warneke, C., Veres, P. R., Roberts, J. M., de Gouw, J. A., Burling, I. R., and Yokelson, R. J.: Biomass burning emissions and potential air quality impacts of volatile organic compounds and other trace gases from fuels common in the US, Atmospheric Chem. Phys., 15, 13915–13938, https://doi.org/10.5194/acp-15-13915-2015, 2015.

Gomez, J., Allen, R. J., Turnock, S. T., Horowitz, L. W., Tsigaridis, K., Bauer, S. E., Olivié, D., Thomson, E. S., and Ginoux, P.: The projected future degradation in air quality is caused by more abundant natural aerosols in a warmer world, Commun. Earth Environ., 4, 1–11, https://doi.org/10.1038/s43247-023-00688-7, 2023.

Gorham, K. A., Raffuse, S. M., Hyslop, N. P., and White, W. H.: Comparison of recent speciated PM2.5 data from collocated CSN and IMPROVE measurements, Atmos. Environ., 244, 117977, https://doi.org/10.1016/j.atmosenv.2020.117977, 2021.

Hallquist, M., Wenger, J. C., Baltensperger, U., Rudich, Y., Simpson, D., Claeys, M., Dommen, J., Donahue, N. M., George, C., Goldstein, A. H., Hamilton, J. F., Herrmann, H., Hoffmann, T., Iinuma, Y., Jang, M., Jenkin, M. E., Jimenez, J. L., Kiendler-Scharr, A., Maenhaut, W., McFiggans, G., Mentel, T. F., Monod, A., Prévôt, A. S. H., Seinfeld, J. H., Surratt, J. D., Szmigielski, R., and Wildt, J.: The formation, properties and impact of secondary organic aerosol: current and emerging issues, Atmospheric Chem. Phys., 9, 5155–5236, https://doi.org/10.5194/acp-9-5155-2009, 2009.

Hand, J. L., Schichtel, B. A., Pitchford, M., Malm, W. C., and Frank, N. H.: Seasonal composition of remote and urban fine particulate matter in the United States, J. Geophys. Res. Atmospheres, 117, https://doi.org/10.1029/2011JD017122, 2012.

Hidy, G. M., Blanchard, C. L., Baumann, K., Edgerton, E., Tanenbaum, S., Shaw, S., Knipping, E., Tombach, I., Jansen, J., and Walters, J.: Chemical climatology of the southeastern United States, 1999–2013, Atmospheric Chem. Phys., 14, 11893–11914, https://doi.org/10.5194/acp-14-11893-2014, 2014.

Jen, C. N., Hatch, L. E., Selimovic, V., Yokelson, R. J., Weber, R., Fernandez, A. E., Kreisberg, N. M., Barsanti, K. C., and Goldstein, A. H.: Speciated and total emission factors of particulate organics from burning western US wildland fuels and their dependence on combustion efficiency, Atmospheric Chem. Phys., 19, 1013–1026, https://doi.org/10.5194/acp-19-1013-2019, 2019.

Kelley, M., Schmidt, G. A., Nazarenko, L. S., Bauer, S. E., Ruedy, R., Russell, G. L., Ackerman, A. S., Aleinov, I., Bauer, M., Bleck, R., Canuto, V., Cesana, G., Cheng, Y., Clune, T. L., Cook, B. I., Cruz, C. A., Del Genio, A. D., Elsaesser, G. S., Faluvegi, G., Kiang, N. Y., Kim, D., Lacis, A. A., Leboissetier, A., LeGrande, A. N., Lo, K. K., Marshall, J., Matthews, E. E., McDermid, S., Mezuman, K., Miller, R. L., Murray, L. T., Oinas, V., Orbe, C., García-Pando, C. P., Perlwitz, J. P., Puma, M. J., Rind, D., Romanou, A., Shindell, D. T., Sun, S., Tausnev, N., Tsigaridis, K., Tselioudis, G., Weng, E., Wu, J., and Yao, M.-S.: GISS-E2.1: Configurations and Climatology, J. Adv. Model. Earth Syst., 12, e2019MS002025, https://doi.org/10.1029/2019MS002025, 2020.

552 Kim, P. S., Jacob, D. J., Fisher, J. A., Travis, K., Yu, K., Zhu, L., Yantosca, R. M., Sulprizio, M. P., Jimenez, J. L.,
553 Campuzano-Jost, P., Froyd, K. D., Liao, J., Hair, J. W., Fenn, M. A., Butler, C. F., Wagner, N. L., Gordon, T. D.,
554 Welti, A., Wennberg, P. O., Crounse, J. D., St. Clair, J. M., Teng, A. P., Millet, D. B., Schwarz, J. P., Markovic, M.
555 Z., and Perring, A. E.: Sources, seasonality, and trends of southeast US aerosol: an integrated analysis of surface,
556 aircraft, and satellite observations with the GEOS-Chem chemical transport model, Atmospheric Chem. Phys., 15,
557 10411–10433, https://doi.org/10.5194/acp-15-10411-2015, 2015.

558 Le Breton, M., Wang, Y., Hallquist, Å. M., Pathak, R. K., Zheng, J., Yang, Y., Shang, D., Glasius, M., Bannan, T.
559 J., Liu, Q., Chan, C. K., Percival, C. J., Zhu, W., Lou, S., Topping, D., Wang, Y., Yu, J., Lu, K., Guo, S., Hu, M.,
560 and Hallquist, M.: Online gas- and particle-phase measurements of organosulfates, organosulfonates and nitrooxy
561 organosulfates in Beijing utilizing a FIGAERO ToF-CIMS, Atmospheric Chem. Phys., 18, 10355–10371,
562 https://doi.org/10.5194/acp-18-10355-2018, 2018.

563 Lee, L. A., Reddington, C. L., and Carslaw, K. S.: On the relationship between aerosol model uncertainty and
564 radiative forcing uncertainty, Proc. Natl. Acad. Sci., 113, 5820–5827, https://doi.org/10.1073/pnas.1507050113,
565 2016.

566 Leeper, R. D., Bilotta, R., Petersen, B., Stiles, C. J., Heim, R., Fuchs, B., Prat, O. P., Palecki, M., and Ansari, S.:
567 Characterizing U.S. drought over the past 20 years using the U.S. drought monitor, Int. J. Climatol., 42, 6616–6630,
568 https://doi.org/10.1002/joc.7653, 2022.

569 Li, W. and Wang, Y.: Reduced surface fine dust under droughts over the southeastern United States during
570 summertime: observations and CMIP6 model simulations, Atmospheric Chem. Phys., 22, 7843–7859,
571 https://doi.org/10.5194/acp-22-7843-2022, 2022.

572 Li, W., Wang, Y., Flynn, J., Griffin, R. J., Guo, F., and Schnell, J. L.: Spatial variation of surface O3 responses to
573 drought over the contiguous United States during summertime: Role of precursor emissions and ozone chemistry, J.
574 Geophys. Res. Atmospheres, 127, e2021JD035607, https://doi.org/10.1029/2021JD035607, 2022.

575 Llusià, J., Peñuelas, J., Alessio, G. A., and Estiarte, M.: Contrasting Species-Specific, Compound-Specific,
576 Seasonal, and Interannual Responses of Foliar Isoprenoid Emissions to Experimental Drought in a Mediterranean
577 Shrubland, Int. J. Plant Sci., 169, 637–645, https://doi.org/10.1086/533603, 2008.

578 Lopez-Hilfiker, F. D., Mohr, C., D'Ambro, E. L., Lutz, A., Riedel, T. P., Gaston, C. J., Iyer, S., Zhang, Z., Gold, A.,
579 Surratt, J. D., Lee, B. H., Kurten, T., Hu, W. W., Jimenez, J., Hallquist, M., and Thornton, J. A.: Molecular
580 composition and volatility of organic aerosol in the southeastern U.S.: Implications for IEPOX derived SOA,
581 Environ. Sci. Technol., 50, 2200–2209, https://doi.org/10.1021/acs.est.5b04769, 2016.

582 Malm, W. C., Schichtel, B. A., Hand, J. L., and Collett Jr., J. L.: Concurrent temporal and spatial trends in sulfate
583 and organic mass concentrations measured in the IMPROVE monitoring program, J. Geophys. Res. Atmospheres,
584 122, 10,462-10,476, https://doi.org/10.1002/2017JD026865, 2017.

585 Maria, S. F., Russell, L. M., Gilles, M. K., and Myneni, S. C. B.: Organic Aerosol Growth Mechanisms and Their
586 Climate-Forcing Implications, Science, 306, 1921–1924, https://doi.org/10.1126/science.1103491, 2004.

587 McClure, C. D. and Jaffe, D. A.: US particulate matter air quality improves except in wildfire-prone areas, Proc.
588 Natl. Acad. Sci., 115, 7901–7906, https://doi.org/10.1073/pnas.1804353115, 2018.

589 NASA: CERES Time-Interpolated TOA Fluxes, Clouds and Aerosols Monthly Terra Edition4A, NASA Langley
590 Atmospheric Science Data Center DAAC [data set],
591 https://doi.org/10.5067/TERRA/CERES/SSF1DEGMONTH_L3.004A, 2015.

592 van Noije, T., Bergman, T., Le Sager, P., O'Donnell, D., Makkonen, R., Gonçalves-Ageitos, M., Döscher, R.,
593 Fladrich, U., von Hardenberg, J., Keskinen, J.-P., Korhonen, H., Laakso, A., Myriokefalitakis, S., Ollinaho, P., Pérez
594 García-Pando, C., Reerink, T., Schrödner, R., Wyser, K., and Yang, S.: EC-Earth3-AerChem: a global climate

595 model with interactive aerosols and atmospheric chemistry participating in CMIP6, Geosci. Model Dev., 14, 5637–
596 5668, https://doi.org/10.5194/gmd-14-5637-2021, 2021.

597 Pegoraro, E., Rey, A., Barron-Gafford, G., Monson, R., Malhi, Y., and Murthy, R.: The interacting effects of
598 elevated atmospheric CO2 concentration, drought and leaf-to-air vapour pressure deficit on ecosystem isoprene
599 fluxes, Oecologia, 146, 120–129, https://doi.org/10.1007/s00442-005-0166-5, 2005.

600 Potosnak, M. J., LeStourgeon, L., Pallardy, S. G., Hosman, K. P., Gu, L., Karl, T., Geron, C., and Guenther, A. B.:
601 Observed and modeled ecosystem isoprene fluxes from an oak-dominated temperate forest and the influence of
602 drought stress, Atmos. Environ., 84, 314–322, https://doi.org/10.1016/j.atmosenv.2013.11.055, 2014.

603 Pye, H. O. T., Murphy, B. N., Xu, L., Ng, N. L., Carlton, A. G., Guo, H., Weber, R., Vasilakos, P., Appel, K. W.,
604 Budisulistiorini, S. H., Surratt, J. D., Nenes, A., Hu, W., Jimenez, J. L., Isaacman-VanWertz, G., Misztal, P. K., and
605 Goldstein, A. H.: On the implications of aerosol liquid water and phase separation for organic aerosol mass,
606 Atmospheric Chem. Phys., 17, 343–369, https://doi.org/10.5194/acp-17-343-2017, 2017.

607 Pye, H. O. T., Ward-Caviness, C. K., Murphy, B. N., Appel, K. W., and Seltzer, K. M.: Secondary organic aerosol
608 association with cardiorespiratory disease mortality in the United States, Nat. Commun., 12, 7215,
609 https://doi.org/10.1038/s41467-021-27484-1, 2021.

610 Randerson, J. T., Chen, Y., van der Werf, G. R., Rogers, B. M., and Morton, D. C.: Global burned area and biomass
611 burning emissions from small fires, J. Geophys. Res. Biogeosciences, 117, https://doi.org/10.1029/2012JG002128,
612 2012.

613 Rasch, P. J., Barth, M. C., Kiehl, J. T., Schwartz, S. E., and Benkovitz, C. M.: A description of the global sulfur
614 cycle and its controlling processes in the National Center for Atmospheric Research Community Climate Model,
615 Version 3, J. Geophys. Res. Atmospheres, 105, 1367–1385, https://doi.org/10.1029/1999JD900777, 2000.

616 Ridley, D. A., Heald, C. L., Ridley, K. J., and Kroll, J. H.: Causes and consequences of decreasing atmospheric
617 organic aerosol in the United States, Proc. Natl. Acad. Sci., 115, 290–295, https://doi.org/10.1073/pnas.1700387115,
618 2018.

619 Riva, M., Tomaz, S., Cui, T., Lin, Y.-H., Perraudin, E., Gold, A., Stone, E. A., Villenave, E., and Surratt, J. D.:
620 Evidence for an Unrecognized Secondary Anthropogenic Source of Organosulfates and Sulfonates: Gas-Phase
621 Oxidation of Polycyclic Aromatic Hydrocarbons in the Presence of Sulfate Aerosol, Environ. Sci. Technol., 49,
622 6654–6664, https://doi.org/10.1021/acs.est.5b00836, 2015.

623 Ruffault, J., Curt, T., Martin-StPaul, N. K., Moron, V., and Trigo, R. M.: Extreme wildfire events are linked to
624 global-change-type droughts in the northern Mediterranean, Nat. Hazards Earth Syst. Sci., 18, 847–856,
625 https://doi.org/10.5194/nhess-18-847-2018, 2018.

626 Scasta, J. D., Weir, J. R., and Stambaugh, M. C.: Droughts and wildfires in western U.S. rangelands, Rangelands,
627 38, 197–203, https://doi.org/10.1016/j.rala.2016.06.003, 2016.

628 Schnell, J. L., Holmes, C. D., Jangam, A., and Prather, M. J.: Skill in forecasting extreme ozone pollution episodes
629 with a global atmospheric chemistry model, Atmospheric Chem. Phys., 14, 7721–7739, https://doi.org/10.5194/acp-
630 14-7721-2014, 2014.

631 Schroder, J. C., Campuzano-Jost, P., Day, D. A., Shah, V., Larson, K., Sommers, J. M., Sullivan, A. P., Campos, T.,
632 Reeves, J. M., Hills, A., Hornbrook, R. S., Blake, N. J., Scheuer, E., Guo, H., Fibiger, D. L., McDuffie, E. E., Hayes,
633 P. L., Weber, R. J., Dibb, J. E., Apel, E. C., Jaeglé, L., Brown, S. S., Thornton, J. A., and Jimenez, J. L.: Sources and
634 secondary production of organic aerosols in the northeastern United States during winter, J. Geophys. Res.
635 Atmospheres, 123, 7771–7796, https://doi.org/10.1029/2018JD028475, 2018.

Séférian, R., Nabat, P., Michou, M., Saint-Martin, D., Voldoire, A., Colin, J., Decharme, B., Delire, C., Berthet, S., Chevallier, M., Sénési, S., Franchisteguy, L., Vial, J., Mallet, M., Joetzjer, E., Geoffroy, O., Guérémy, J.-F., Moine, M.-P., Msadek, R., Ribes, A., Rocher, M., Roehrig, R., Salas-y-Mélia, D., Sanchez, E., Terray, L., Valcke, S., Waldman, R., Aumont, O., Bopp, L., Deshayes, J., Éthé, C., and Madec, G.: Evaluation of CNRM Earth System Model, CNRM-ESM2-1: Role of Earth System Processes in Present-Day and Future Climate, J. Adv. Model. Earth Syst., 11, 4182–4227, https://doi.org/10.1029/2019MS001791, 2019.

Seland, Ø., Bentsen, M., Olivié, D., Toniazzo, T., Gjermundsen, A., Graff, L. S., Debernard, J. B., Gupta, A. K., He, Y.-C., Kirkevåg, A., Schwinger, J., Tjiputra, J., Aas, K. S., Bethke, I., Fan, Y., Griesfeller, J., Grini, A., Guo, C., Ilicak, M., Karset, I. H. H., Landgren, O., Liakka, J., Moseid, K. O., Nummelin, A., Spensberger, C., Tang, H., Zhang, Z., Heinze, C., Iversen, T., and Schulz, M.: Overview of the Norwegian Earth System Model (NorESM2) and key climate response of CMIP6 DECK, historical, and scenario simulations, Geosci. Model Dev., 13, 6165–6200, https://doi.org/10.5194/gmd-13-6165-2020, 2020.

Senior, C. A., Jones, C. G., Wood, R. A., Sellar, A., Belcher, S., Klein-Tank, A., Sutton, R., Walton, J., Lawrence, B., Andrews, T., and Mulcahy, J. P.: U.K. Community Earth System Modeling for CMIP6, J. Adv. Model. Earth Syst., 12, e2019MS002004, https://doi.org/10.1029/2019MS002004, 2020.

Shrivastava, M., Cappa, C. D., Fan, J., Goldstein, A. H., Guenther, A. B., Jimenez, J. L., Kuang, C., Laskin, A., Martin, S. T., Ng, N. L., Petaja, T., Pierce, J. R., Rasch, P. J., Roldin, P., Seinfeld, J. H., Shilling, J., Smith, J. N., Thornton, J. A., Volkamer, R., Wang, J., Worsnop, D. R., Zaveri, R. A., Zelenyuk, A., and Zhang, Q.: Recent advances in understanding secondary organic aerosol: Implications for global climate forcing, Rev. Geophys., 55, 509–559, https://doi.org/10.1002/2016RG000540, 2017.

Strzepek, K., Yohe, G., Neumann, J., and Boehlert, B.: Characterizing changes in drought risk for the United States from climate change, Environ. Res. Lett., 5, 044012, https://doi.org/10.1088/1748-9326/5/4/044012, 2010.

Surratt, J. D., Chan, A. W. H., Eddingsaas, N. C., Chan, M., Loza, C. L., Kwan, A. J., Hersey, S. P., Flagan, R. C., Wennberg, P. O., and Seinfeld, J. H.: Reactive intermediates revealed in secondary organic aerosol formation from isoprene, Proc. Natl. Acad. Sci., 107, 6640–6645, https://doi.org/10.1073/pnas.0911114107, 2010.

Tai, A. P. K., Mickley, L. J., and Jacob, D. J.: Correlations between fine particulate matter (PM2.5) and meteorological variables in the United States: Implications for the sensitivity of PM2.5 to climate change, Atmos. Environ., 44, 3976–3984, https://doi.org/10.1016/j.atmosenv.2010.06.060, 2010.

Tatebe, H., Ogura, T., Nitta, T., Komuro, Y., Ogochi, K., Takemura, T., Sudo, K., Sekiguchi, M., Abe, M., Saito, F., Chikira, M., Watanabe, S., Mori, M., Hirota, N., Kawatani, Y., Mochizuki, T., Yoshimura, K., Takata, K., O'ishi, R., Yamazaki, D., Suzuki, T., Kurogi, M., Kataoka, T., Watanabe, M., and Kimoto, M.: Description and basic evaluation of simulated mean state, internal variability, and climate sensitivity in MIROC6, Geosci. Model Dev., 12, 2727–2765, https://doi.org/10.5194/gmd-12-2727-2019, 2019.

Taufik, M., Torfs, P. J. J. F., Uijlenhoet, R., Jones, P. D., Murdiyarso, D., and Van Lanen, H. A. J.: Amplification of wildfire area burnt by hydrological drought in the humid tropics, Nat. Clim. Change, 7, 428–431, https://doi.org/10.1038/nclimate3280, 2017.

Thornhill, G., Collins, W., Olivié, D., Skeie, R. B., Archibald, A., Bauer, S., Checa-Garcia, R., Fiedler, S., Folberth, G., Gjermundsen, A., Horowitz, L., Lamarque, J.-F., Michou, M., Mulcahy, J., Nabat, P., Naik, V., O'Connor, F. M., Paulot, F., Schulz, M., Scott, C. E., Séférian, R., Smith, C., Takemura, T., Tilmes, S., Tsigaridis, K., and Weber, J.: Climate-driven chemistry and aerosol feedbacks in CMIP6 Earth system models, Atmospheric Chem. Phys., 21, 1105–1126, https://doi.org/10.5194/acp-21-1105-2021, 2021.

Tsui, W. G., Woo, J. L., and McNeill, V. F.: Impact of Aerosol-Cloud Cycling on Aqueous Secondary Organic Aerosol Formation, Atmosphere, 10, 666, https://doi.org/10.3390/atmos10110666, 2019.

679 Turnock, S. T., Allen, R. J., Andrews, M., Bauer, S. E., Deushi, M., Emmons, L., Good, P., Horowitz, L., John, J.
680 G., Michou, M., Nabat, P., Naik, V., Neubauer, D., O'Connor, F. M., Olivié, D., Oshima, N., Schulz, M., Sellar, A.,
681 Shim, S., Takemura, T., Tilmes, S., Tsigaridis, K., Wu, T., and Zhang, J.: Historical and future changes in air
682 pollutants from CMIP6 models, Atmospheric Chem. Phys., 20, 14547–14579, https://doi.org/10.5194/acp-20-
683 14547-2020, 2020.

684 Vicente-Serrano, S. M., Beguería, S., and López-Moreno, J. I.: A multiscalar drought index sensitive to global
685 warming: The Standardized Precipitation Evapotranspiration Index, J. Clim., 23, 1696–1718,
686 https://doi.org/10.1175/2009JCLI2909.1, 2010.

687 Wang, Y., Xie, Y., Cai, L., Dong, W., Zhang, Q., and Zhang, L.: Impact of the 2011 southern U.S. drought on
688 ground-level fine aerosol concentration in summertime, J. Atmospheric Sci., 72, 1075–1093,
689 https://doi.org/10.1175/JAS-D-14-0197.1, 2015.

690 Wang, Y., Xie, Y., Dong, W., Ming, Y., Wang, J., and Shen, L.: Adverse effects of increasing drought on air quality
691 via natural processes, Atmospheric Chem. Phys., 17, 12827–12843, https://doi.org/10.5194/acp-17-12827-2017,
692 2017.

693 Wang, Y., Wang, J., Wang, Y., and Li, W.: Drought impacts on PM2.5 composition and amount over the US during
694 1988–2018, J. Geophys. Res. Atmospheres, 127, e2022JD037677, https://doi.org/10.1029/2022JD037677, 2022a.

695 Wang, Y., Lin, N., Li, W., Guenther, A., Lam, J. C. Y., Tai, A. P. K., Potosnak, M. J., and Seco, R.: Satellite-
696 derived constraints on the effect of drought stress on biogenic isoprene emissions in the southeastern US,
697 Atmospheric Chem. Phys., 22, 14189–14208, https://doi.org/10.5194/acp-22-14189-2022, 2022b.

698 Wilhite, D. A., Svoboda, M. D., and Hayes, M. J.: Understanding the complex impacts of drought: A key to
699 enhancing drought mitigation and preparedness, Water Resour. Manag., 21, 763–774,
700 https://doi.org/10.1007/s11269-006-9076-5, 2007.

701 Wu, C., Pullinen, I., Andres, S., Carriero, G., Fares, S., Goldbach, H., Hacker, L., Kasal, T., Kiendler-Scharr, A.,
702 Kleist, E., Paoletti, E., Wahner, A., Wildt, J., and Mentel, T. F.: Impacts of soil moisture on de novo monoterpene
703 emissions from European beech, Holm oak, Scots pine, and Norway spruce, Biogeosciences, 12, 177–191,
704 https://doi.org/10.5194/bg-12-177-2015, 2015.

705 Wu, T., Zhang, F., Zhang, J., Jie, W., Zhang, Y., Wu, F., Li, L., Yan, J., Liu, X., Lu, X., Tan, H., Zhang, L., Wang,
706 J., and Hu, A.: Beijing Climate Center Earth System Model version 1 (BCC-ESM1): model description and
707 evaluation of aerosol simulations, Geosci. Model Dev., 13, 977–1005, https://doi.org/10.5194/gmd-13-977-2020,
708 2020.

709 Xie, Y., Wang, Y., Dong, W., Wright, J. S., Shen, L., and Zhao, Z.: Evaluating the response of summertime surface
710 sulfate to hydroclimate variations in the continental United States: Role of meteorological inputs in the GEOS-Chem
711 model, J. Geophys. Res. Atmospheres, 124, 1662–1679, https://doi.org/10.1029/2018JD029693, 2019.

712 Xu, L., Guo, H., Boyd, C. M., Klein, M., Bougiatioti, A., Cerully, K. M., Hite, J. R., Isaacman-VanWertz, G.,
713 Kreisberg, N. M., and Knote, C.: Effects of anthropogenic emissions on aerosol formation from isoprene and
714 monoterpenes in the southeastern United States, Proc. Natl. Acad. Sci., 112, 37–42, 2015.

715 Yli-Juuti, T., Mielonen, T., Heikkinen, L., Arola, A., Ehn, M., Isokääntä, S., Keskinen, H.-M., Kulmala, M., Laakso,
716 A., Lipponen, A., Luoma, K., Mikkonen, S., Nieminen, T., Paasonen, P., Petäjä, T., Romakkaniemi, S., Tonttila, J.,
717 Kokkola, H., and Virtanen, A.: Significance of the organic aerosol driven climate feedback in the boreal area, Nat.
718 Commun., 12, 5637, https://doi.org/10.1038/s41467-021-25850-7, 2021.

719 Yukimoto, S., Kawai, H., Koshiro, T., Oshima, N., Yoshida, K., Urakawa, S., Tsujino, H., Deushi, M., Tanaka, T.,
720 Hosaka, M., Yabu, S., Yoshimura, H., Shindo, E., Mizuta, R., Obata, A., Adachi, Y., and Ishii, M.: The
721 Meteorological Research Institute Earth System Model Version 2.0, MRI-ESM2.0: Description and Basic

Evaluation of the Physical Component, J. Meteorol. Soc. Jpn. Ser II, 97, 931–965, https://doi.org/10.2151/jmsj.2019-051, 2019.

Zhang, Q., Jimenez, J. L., Canagaratna, M. R., Ulbrich, I. M., Ng, N. L., Worsnop, D. R., and Sun, Y.: Understanding atmospheric organic aerosols via factor analysis of aerosol mass spectrometry: a review, Anal. Bioanal. Chem., 401, 3045–3067, https://doi.org/10.1007/s00216-011-5355-y, 2011.

Zhang, X., Liu, Z., Hecobian, A., Zheng, M., Frank, N. H., Edgerton, E. S., and Weber, R. J.: Spatial and seasonal variations of fine particle water-soluble organic carbon (WSOC) over the southeastern United States: implications for secondary organic aerosol formation, Atmospheric Chem. Phys., 12, 6593–6607, https://doi.org/10.5194/acp-12-6593-2012, 2012.

Zhao, Z., Wang, Y., Qin, M., Hu, Y., Xie, Y., and Russell, A. G.: Drought impacts on secondary organic aerosol: a case study in the southeast United States, Environ. Sci. Technol., 53, 242–250, https://doi.org/10.1021/acs.est.8b04842, 2019.

Zheng, Y., Thornton, J. A., Ng, N. L., Cao, H., Henze, D. K., McDuffie, E. E., Hu, W., Jimenez, J. L., Marais, E. A., Edgerton, E., and Mao, J.: Long-term observational constraints of organic aerosol dependence on inorganic species in the southeast US, Atmospheric Chem. Phys., 20, 13091–13107, https://doi.org/10.5194/acp-20-13091-2020, 2020.